

COMMUNICATION

Structural Analysis of Peroxide-Soaked MnSOD Crystals Reveals Side-On Binding of Peroxide to Active-Site Manganese

Jason Porta^{1,2}, Ardeschir Vahedi-Faridi³ and Gloria E. O. Borgstahl^{1*}

¹The Eppley Institute for Research in Cancer and Allied Diseases, 987696 Nebraska Medical Center, Omaha, NE 68198-7696, USA

²Department of Biochemistry and Molecular Biology, 987696 Nebraska Medical Center, Omaha, NE 68198-7696, USA

³Department of Chemistry, The University of Toledo, 2801 West Bancroft Street, Toledo, OH 43606, USA

Received 24 November 2009;
received in revised form
24 February 2010;
accepted 18 April 2010
Available online
24 April 2010

The superoxide dismutase (SOD) enzymes are important antioxidant agents that protect cells from reactive oxygen species. The SOD family is responsible for catalyzing the disproportionation of superoxide radical to oxygen and hydrogen peroxide. Manganese- and iron-containing SOD exhibit product inhibition whereas Cu/ZnSOD does not. Here, we report the crystal structure of *Escherichia coli* MnSOD with hydrogen peroxide cryotrapped in the active site. Crystallographic refinement to 1.55 Å and close inspection revealed electron density for hydrogen peroxide in three of the four active sites in the asymmetric unit. The hydrogen peroxide molecules are in the position opposite His26 that is normally assumed by water in the trigonal bipyramidal resting state of the enzyme. Hydrogen peroxide is present in active sites B, C, and D and is side-on coordinated to the active-site manganese. In chains B and D, the peroxide is oriented in the plane formed by manganese and ligands Asp167 and His26. In chain C, the peroxide is bound, making a 70° angle to the plane. Comparison of the peroxide-bound active site with the hydroxide-bound octahedral form shows a shifting of residue Tyr34 towards the active site when peroxide is bound. Comparison with peroxide-soaked Cu/ZnSOD indicates end-on binding of peroxide when the SOD does not exhibit inhibition by peroxide and side-on binding of peroxide in the product-inhibited state of MnSOD.

© 2010 Elsevier Ltd. All rights reserved.

Edited by M. Guss

Keywords: manganese superoxide dismutase; X-ray crystallography; hydrogen peroxide; side-on binding; product inhibition

Superoxide dismutases (SODs) are important antioxidant enzymes that protect against toxic oxygen metabolites and are found in all cells. The *sod1* gene codes for the cytoplasmic copper/zinc forms, *sod2* codes for the mitochondrial manganese form, and *sod3* codes for the secreted extracellular form.¹ Defects in SODs are relevant to brain pathology, cancer, and other late-onset diseases.² For example, mutations in SOD are associated with

the inherited form of amyotrophic lateral sclerosis, or Lou Gehrig's disease, a fatal neurodegenerative disorder.^{3,4}

The MnSODs from bacteria are homologous to human SODs and have similar monomeric folds and practically identical active-site geometries.^{5–7} MnSODs can be either homodimers or homotetramers, where each subunit has a molecular mass of ~22 kDa. *Escherichia coli* MnSOD, as well as the homologous FeSOD, functions as a homodimer (as shown in Fig. 1a). Human MnSOD functions as a tetramer. Each MnSOD subunit is composed of two domains, which flank the active-site manganese (Fig. 1b). The N-terminal domain contains two α -helices and the C-terminal domain contains four α -helices and a three-stranded antiparallel β -sheet. Each domain contributes ligands that coordinate to the active-site manganese. His26 and His81 from the

*Corresponding author. E-mail address: gborgstahl@unmc.edu.

Present address: A. Vahedi-Faridi, Old Dominion University Research Foundation, 4111 Monarch Way, Norfolk, VA 23508, USA.

Abbreviations used: SOD, superoxide dismutase; PDB, Protein Data Bank.

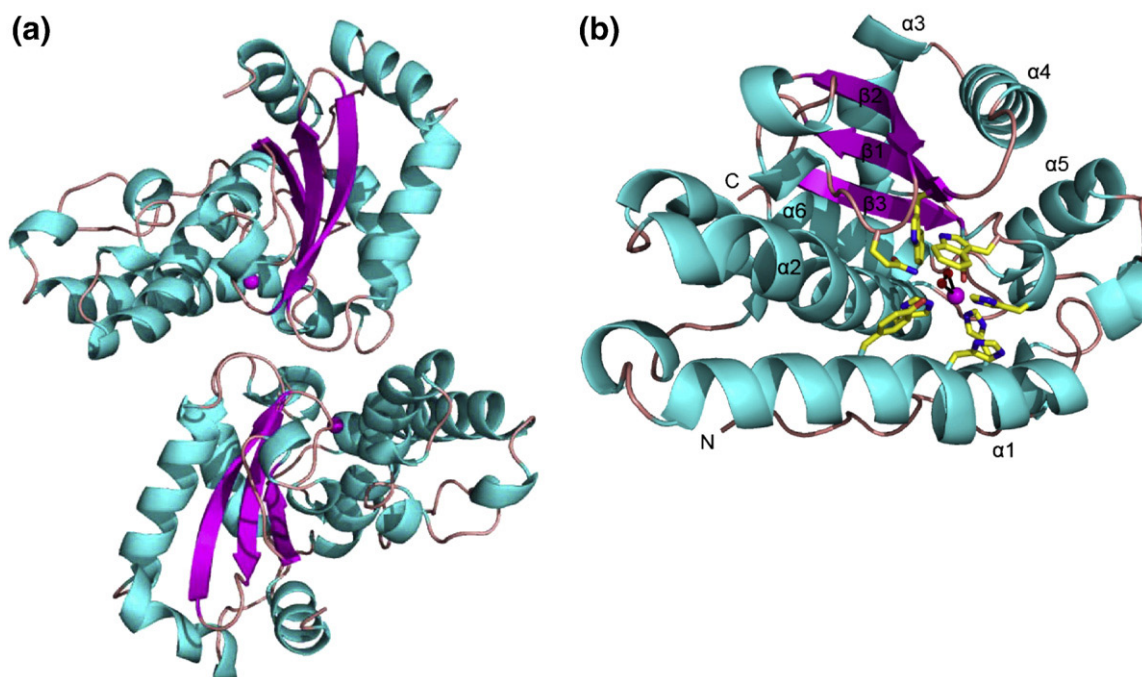


Fig. 1. MnSOD ribbon diagrams. (a) MnSOD homodimer; the active-site manganese is pink, α -helices are cyan, and β -strands are magenta. (b) Individual monomer (chain B) with active-site manganese, bound peroxide, and active-site residues (oxygen, red; nitrogen, blue; carbon, yellow). Secondary structural units, including α -helices, β -strands, and N- and C-termini, are labeled.

N-terminal domain and Asp167 and His171 from the C-terminal domain are covalently bound to the active-site manganese. In the resting state, the active site has a distorted trigonal bipyramidal geometry with a water molecule in the fifth position (opposite His26 in Fig. 2d). MnSOD and FeSOD inhibitors such as sodium azide and hydroxide bind to the manganese in the sixth position (opposite Asp167 in Fig. 2a) in a distorted octahedral geometry.

SODs are characterized as some of the fastest known enzymes with a k_{cat}/K_m of $10^{-9} \text{ M}^{-1} \text{ s}^{-1}$ and are rate-limited only by the diffusion of their substrates and products.⁸ SOD catalyzes the dis-

mutation of superoxide to oxygen and hydrogen peroxide, utilizing a reaction mechanism that involves the cyclic transition of the metal ion between the trivalent and divalent state as they oxidize their substrate.⁹ MnSOD exhibits strong product inhibition whereas Cu/ZnSOD does not.¹⁰⁻¹⁴

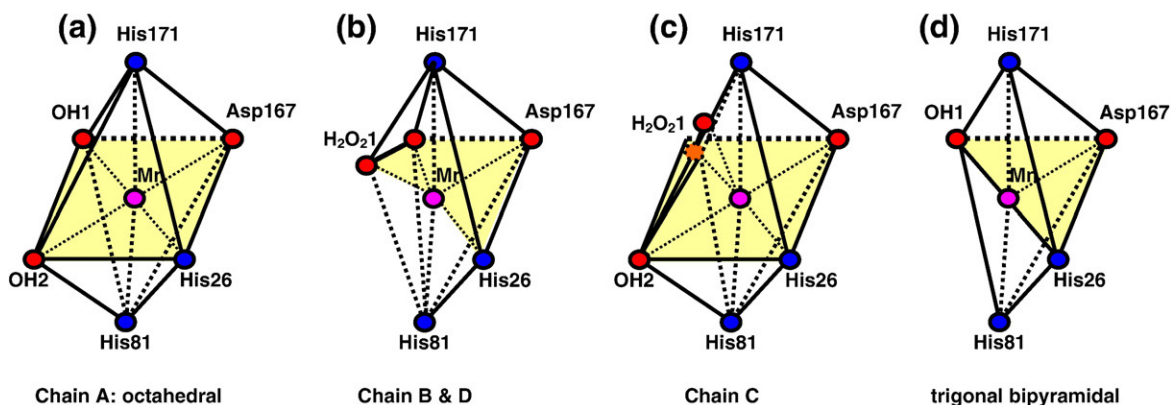
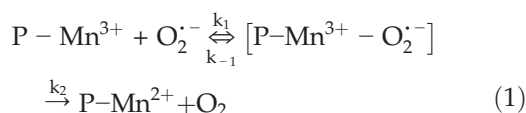
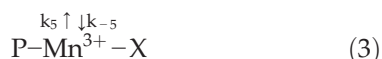
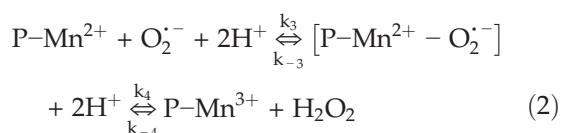


Fig. 2. Schematics of MnSOD coordination states found in peroxide-soaked crystals (a–c) and the normal resting state (d). (a) Chain A contained a six-coordinate octahedral active site with two hydroxides bound. (b) Chains B and D contained one peroxide bound in the plane with Asp167 and His26. (c) In chain C, the hydrogen peroxide is bound at an angle to the plane and hydroxide is observed in the second position. (d) The five-coordinate trigonal bipyramidal coordination state found in most crystal structures.



Here, P-Mn represents the protein bound to metal in the trigonal bipyramidal geometry. The product-inhibited form of the enzyme is represented as P-Mn³⁺-X in Eq. (3).

One proposed reaction mechanism based on crystal structure analysis and X-ray absorption studies suggests that superoxide coordinates to the metal atom and becomes oxidized to hydrogen peroxide in a two-step mechanism, during which the coordination state of the active site goes from five-coordinate trigonal bipyramidal to six-coordinate octahedral and back to five-coordinate (5-6-5 mechanism) again.¹⁵⁻¹⁷ It was also concluded that anionic inhibitors bind in the same orientation (end-on) and position (sixth) as the substrate superoxide. A second mechanism, called associative displacement, was proposed from studies on temperature-dependent absorption or thermochromism of anion complexes.¹⁸ It is believed that in this mechanism, six-coordinate anionic complexes represent an inactive form of the enzyme, and in the active form, the metal ion is always five-coordinate, with anion binding displacing one of the manganese ligands (bound water or Asp167). This study on the binding of peroxide to the active site should show how product can inhibit the enzyme and shed some light on the mechanism employed by MnSOD.

Due to the fast catalytic rate of SOD enzymes, it has proven difficult to trap reaction intermediates of SOD. Inhibitory hydroxide binding to MnSOD was observed by cryotrapping.¹⁹ More recently, a cryotrapped peroxide binding to Cu/ZnSOD reported end-on binding of peroxide to the active-site copper.²⁰ In this study, we have applied these cryotrapping techniques to solve the structure of *E. coli* MnSOD with bound peroxide. We were able to trap peroxide in the active site of MnSOD and visualized side-on binding of peroxide to the active-site manganese. The peroxide displaced the water normally bound to manganese.

For the structure determination of peroxide-bound MnSOD, cryocooled synchrotron diffraction data from a crystal soaked in reservoir solution containing 20% glycerol and 0.008% peroxide were collected (Table 1). The structure was solved using the complementary, non-soaked, cryocooled structure solved previously [1D5N] that contained two hydroxides in a distorted octahedral active site due to the pH used for crystal growth (pH 8.5).¹⁹ All solvent and active-site metals were removed from the starting coordinates, and simple molecular replacement was done by rigid-body refinement followed by restrained-positional refinement using Refmac to 1.55 Å resolution.²² The protein model was compared to omit electron density maps and fit.

Table 1. Diffraction data and refinement statistics

A. Data	
Space group	C222 ₁
Unit cell dimensions (Å)	<i>a</i> = 100.85, <i>b</i> = 107.42, <i>c</i> = 180.04
Resolution range (Å)	50–1.55
No. of unique reflections	135,945
Average redundancy	8.5
Completeness (%)	96.4 (82.0)
<i>I</i> / σ	22.0 (2.2)
<i>R</i> _{sym} (%)	5.8 (43.4)
B. Refinement	
Contents of model	
Protein	4 × 205 amino acid residues
Manganese	4
Hydrogen peroxide molecules	3
Hydroxide ligands	6
Water molecules	492
Geometry	
r.m.s.d. bonds (Å)	0.011
r.m.s.d. angles (°)	1.339
X-ray data (%)	
<i>R</i> -factor (20–1.55 Å)	22.7
<i>R</i> _{free} (20–1.55 Å)	27.0
Average <i>B</i> -factors (Å ²)	
Protein	6.83
Manganese	2.75
Hydroxide/Peroxide	3.14
Water	9.31

E. coli MnSOD crystals were grown as previously described¹⁹ and then soaked in reservoir solution containing 20% glycerol and 0.008% hydrogen peroxide for 1 h. The crystal was mounted on a loop and flash-cooled in a nitrogen stream at 100 K. Diffraction data were collected at Stanford Synchrotron Radiation Lightsource beamline 7-1 in April 2001 with $\lambda = 1.08$ Å using a Mar345 detector and were processed using HKL2000.²¹ $R_{\text{sym}} = \sum_{hkl} |I_{hkl} - \langle I_{hkl} \rangle| / \sum_{hkl} I_{hkl}$. Refinement was carried out using Refmac5.5.²² The 1.55-Å structure of *E. coli* MnSOD (1D5N) was used as a starting model.¹⁹ All solvent and manganese atoms were initially removed from the structure, and the initial *R* value was 47.3%. The *R* value was decreased by iterative cycles of rigid-body refinement where the resolution was increased in steps (*R* = 37.5% and *R*_{free} = 40.2%). The structure was then subjected to 20 cycles of restrained refinement to 1.55 Å. *F*_o - *F*_c maps showed density for manganese in each of the four active sites. Manganese was therefore added to each active site and then subjected to another 20 cycles of restrained refinement. Following refinement, active sites B, C, and D showed density for Mn-bound hydrogen peroxide. Partially occupied peroxides and hydroxide were then added to the active sites followed by another round of restrained refinement. Ramachandran analysis in Procheck indicates that 90.9% and 7.5% of residues fall within the sterically most favored regions and additional allowed regions of a Ramachandran plot, respectively.²³ Side chains in the region 101–110 displayed poor electron density in chain B, but these side chains were retained in the model.

Completely new solvent structure was modeled with Coot,²⁴ and active-site manganese ions with their covalently bound peroxide and/or hydroxide ligands were modeled by-hand into omit electron density maps (Fig. 3; Table 1). Due to cryocooling and diffraction that extended beyond the edge of the X-ray detector, the protein atoms have low mobility with a mean *B*-factor of 7.5 Å². Water molecules have an average *B*-factor of 6.3 Å². The active sites were very well ordered with average *B*-factors of 1.9 and 3.9 Å² for the manganese and hydrogen peroxide, respectively. In the last stages of refinement, anisotropic temperature factors were refined

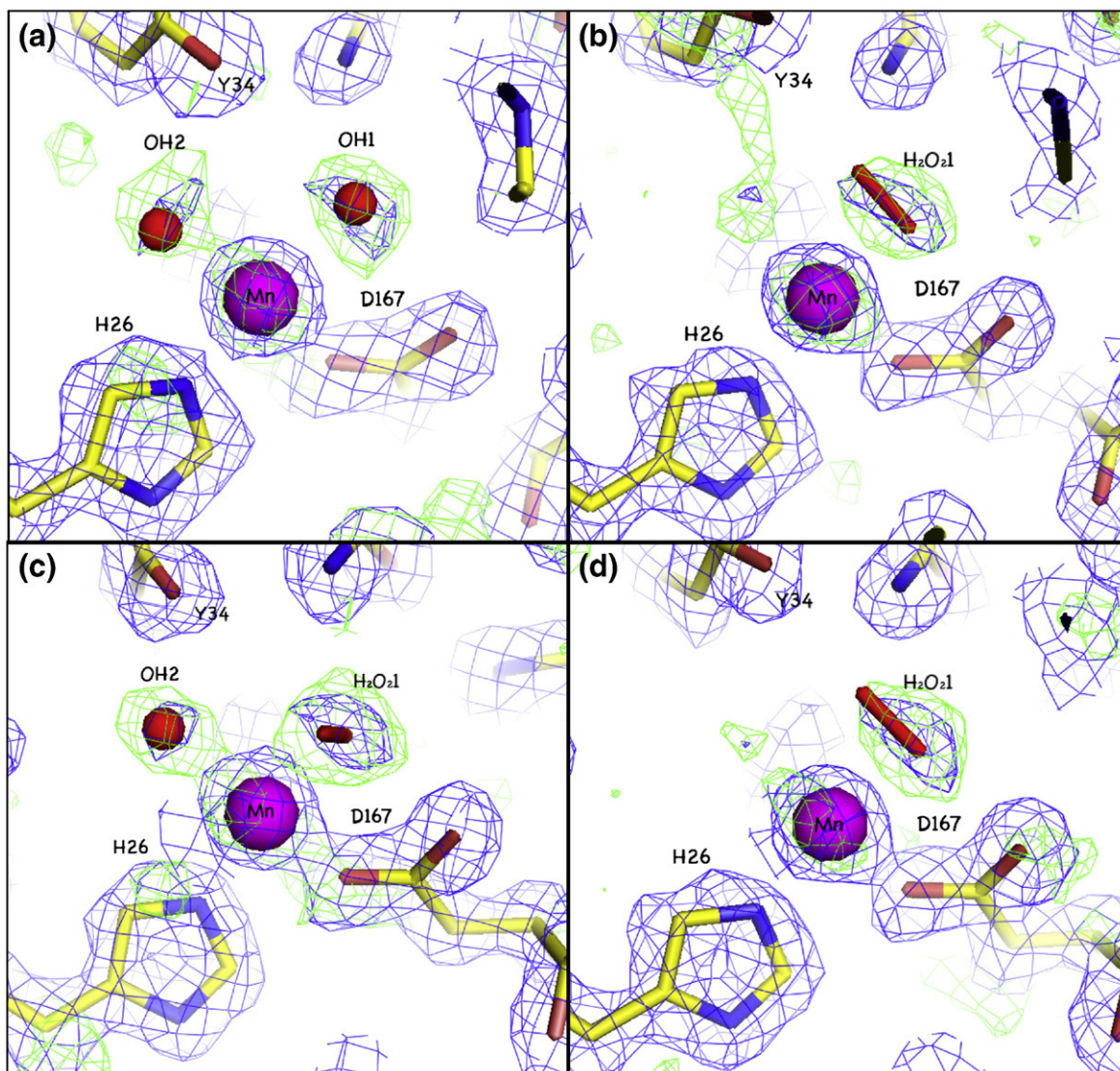


Fig. 3. Peroxide-soaked MnSOD active-site model and electron density. (a) Chain A, (b) chain B, (c) chain C, and (d) chain D. Omit maps were calculated to remove phase bias as follows. First, the manganese and bound solvent were omitted from the structure, and then the structure was randomly distorted by 0.1 Å using Moleman2 software²⁵ followed by positional refinement and map calculation by Refmac. Omit maps were calculated with Fourier coefficients $F_o - F_c$ in green, and $2F_o - F_c$ density is in blue.

and the occupancies of manganese ligands (H_2O_2 and OH) were varied manually to obtain reasonable, refined B -factors between bonded atoms and a flat $F_o - F_c$ electron density map.

This crystal form of *E. coli* MnSOD has two homodimers in the crystallographic asymmetric unit, and this provides four atomic views of the manganese-containing active site.¹⁹ The active site varied in ligand composition as summarized in Fig. 2a–c. In active site A, two hydroxide ligands were modeled as was found in the complementary, non-soaked structure (PDB code 1D5N). Partially occupied peroxide/hydroxide was modeled in active sites B, C, and D when the electron density had a “baking potato-like” ellipsoid shape (Fig. 3). More electron density was observed near oxygen O1 of the peroxide and the B -factors of the

two peroxide oxygens did not refine equivalently; hence, it was decided that a partially occupied hydroxide probably resides in that position and was modeled and refined. For active site C, the sixth ligand position was modeled with hydroxide (OH2, Fig. 2c), but the electron density for chains B and D was judged to be too poorly occupied to justify modeling a ligand although some residual density was observed (Fig. 3).

In three out of four active sites, one hydrogen peroxide molecule H_2O_2 1 is side-on bound to the active-site manganese in the position normally occupied by an active-site water or hydroxide. The peroxide molecule is neighbored by outer shell residues Tyr34, Gln146, and Trp169 (Fig. 4). Trp169 forms a hydrophobic side of the active-site cavity of MnSOD. The peroxide lies in a position that is

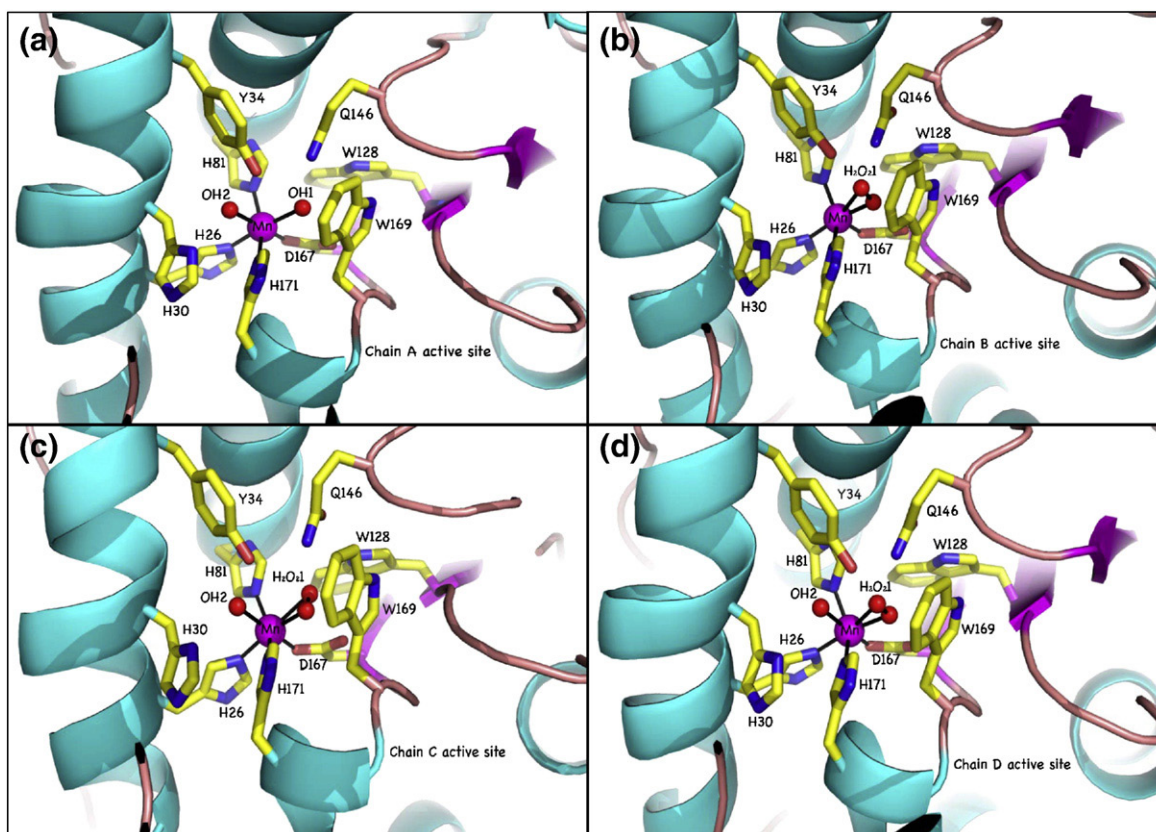


Fig. 4. Active-site view of each subunit. (a) Chain A, (b) chain B, (c) chain C, and (d) chain D. Manganese ion (pink); α -helices (cyan); β -strands (pink); bound hydroxide or peroxide (red); bound His26, His81, Asp167, and His171 ligands; and second shell residues His30, Tyr34, Trp128, Gln146, and Trp169 (carbon yellow, nitrogen blue, oxygen red) are shown.

parallel to Trp169 and is in hydrogen-bond distance with $N^{\epsilon 2}$ of Gln146 and $O^{\delta 1}$ of Asp167. In chains B and D, the peroxide lies in the plane with the

manganese, $N^{\epsilon 2}$ of His26, and $O^{\delta 2}$ of Asp167 and is in hydrogen-bond distance with OH of Tyr34 (Table 2). In chain C, the presumably inhibitory hydroxide is

Table 2. Active-site geometry^a

	Chain A	Chain B	Chain C	Chain D	1D5N ^b
A. Covalent bonds (\AA)					
Mn-His26($N^{\epsilon 2}$)	2.06	2.10	2.09	2.06	2.19 (0.03)
Mn-His81($N^{\epsilon 2}$)	2.07	2.08	2.09	2.07	2.19 (0.02)
Mn-Asp167($O^{\delta 2}$)	1.95	1.95	1.94	1.95	2.04 (0.04)
Mn-His171($N^{\epsilon 2}$)	2.11	2.07	2.09	2.07	2.19 (0.01)
Mn-OH1(O) ^c	2.23	2.11	2.25	2.21	2.19 (0.02)
Mn-OH2(O)	2.37		2.35		2.42 (0.01)
Mn-H ₂ O ₂ 1(O1) ^a		2.09	2.09	2.09	
Mn-H ₂ O ₂ 1(O2)		2.58	2.10	2.49	
B. Hydrogen bonds (\AA)					
OH1(O)-Gln146($N^{\epsilon 2}$) ^c	2.67	2.85	2.94	2.89	2.89 (0.04)
OH1(O)-Asp167($O^{\delta 1}$) ^c	2.98	2.89	2.64	2.72	2.83 (0.08)
OH2(O)-Tyr34(OH)	3.02		2.40		3.43 (0.23)
H ₂ O ₂ 1(O1)-Asp167($O^{\delta 1}$) ^c		2.58	2.94	2.54	
H ₂ O ₂ 1(O2)-Gln146($N^{\epsilon 2}$)		2.42	3.04	2.24	
H ₂ O ₂ 1(O2)-Tyr34(OH)		3.19	4.08	2.83	
Gln146($N^{\epsilon 1}$)-Tyr34(OH)	2.85	2.97	2.89	2.68	2.94 (0.02)
Gln146($O^{\epsilon 1}$)-Asn80($N^{\epsilon 2}$)	3.17	3.13	3.29	3.39	3.25 (0.08)
Gln146($O^{\epsilon 1}$)-Trp128($N^{\epsilon 1}$)	2.90	2.86	2.87	2.85	2.97 (0.01)

^a The corresponding residues between *E. coli* and human MnSOD are as follows: His26=His26, Tyr34=Tyr34, Asn80=Asn73, His81=His74, Trp128=Trp123, Gln146=Gln143, Asp167=Asp159, and His171=His163.

^b For 1D5N, a 100 K *E. coli* MnSOD structure with two hydroxides in the distorted octahedral active site; the average of all four active sites is given with the standard deviation in parentheses.

^c In chains B, C, and D, the peroxide atom H₂O₂1(O1) and hydroxide atom OH1(O) are partially occupied and reside in the same position in the active site.

in the sixth position and the peroxide is at an $\sim 70^\circ$ angle to the Mn-His26-Asp167 plane and the bond to OH of Tyr34 is stretched to $>4 \text{ \AA}$. Thus, in chain C, the bond to OH of Tyr34 is broken and is not replaced with another hydrogen bond.

Most of the features of the peroxide-soaked structure are similar to the non-soaked counterpart (Fig. 5) with the six-coordinate octahedral active site. The C^α atoms of the polypeptide chain were superimposed in order to compare these two structures. This comparison shows that upon peroxide binding, there are no major global changes taking place, but rather small changes in active-site geometry. The largest movement is that of the OH of Tyr34, which shifted 0.9 \AA towards the bound hydroxide OH2 and peroxide in chain C.

Side-on binding of peroxide to manganese is observed in three out of four active sites in the crystallographic asymmetric unit. There is precedence for side-on binding of peroxide to manganese in several model compound crystal structures.^{26,27} The observation of side-on binding of peroxide to MnSOD is very different from the end-on binding of azide to FeSOD. Inhibitory azide binding is also different in that it binds to the sixth position of the active-site metal whereas

we observe peroxide displacing the active-site water in the fifth position.¹⁵ It is also different from the end-on peroxide binding to Cu/ZnSOD.²⁰ With these structural differences, it is noteworthy that MnSOD exhibits product inhibition whereas Cu/ZnSOD does not (excluding Fenton effects).^{11–14} MnSOD is strongly product inhibited, and earlier kinetic studies on MnSOD assigned the inactive form of the enzyme to characteristic bands near 650 and 410 nm.¹¹ This inactivation was speculated to occur by oxidative addition of superoxide to Mn(II), within a Michaelis complex, forming a cyclic peroxo complex of Mn(III). Adding peroxide to MnSOD gives a visible absorption spectrum identical with the product-inhibited complex.¹³ Therefore, the side-on peroxide structure determined here most likely represents this inhibited state of the enzyme.

The peroxide molecule is surrounded by outer shell residues Tyr34, Gln146, and Trp169. Interestingly, mutation of Tyr34 to Phe results in negligible changes in active-site structure, in enhanced product inhibition during the catalysis of superoxide dismutation, and in a slower rate of decay of the P-Mn³⁺-X complex in Eq. (3).^{13,28} The peroxide is next to Trp169, which forms a

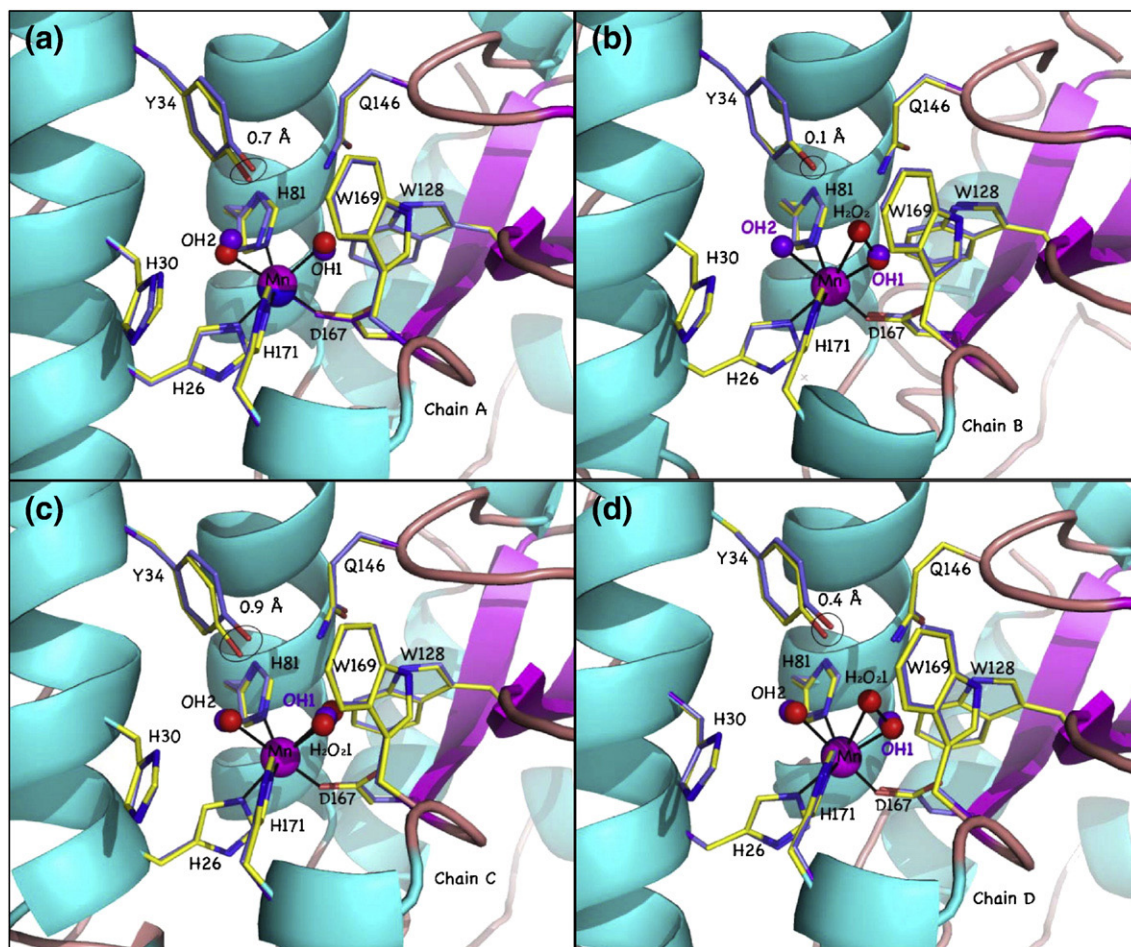


Fig. 5. Comparison of cryotrapped peroxide-soaked (present study) with cryotrapped hydroxide-bound MnSOD (1D5N active-site residues are denoted in purple sticks and spheres. Movement of the Y34 OH is given.

hydrophobic side for the active-site cavity of MnSOD. When Trp169 is mutated to Phe, the enzyme becomes highly product inhibited.²⁹ Mutation of Trp169 to Ala causes significant structural conformational changes to Gln143 and Tyr34, causes the catalysis to decrease by at least 100-fold, and promotes a competing pathway leading to product inhibition.¹² These observed increases in product inhibition when the neighbors of the peroxide are mutated are consistent with this as the true location of the bound peroxide.

Peroxide binding causes a motion of Tyr34 towards the active site. It is known that dissociation of the product-inhibited complex involves proton transfer, but the source of the protons is still unclear.¹² There is some evidence suggesting that Tyr34 is not a proton donor promoting the dissociation of the product-inhibited complex.³⁰ The motion of Tyr34 towards the peroxide is consistent with improved hydrogen bonding to the active site when peroxide is bound.

In conclusion, the structure of peroxide-bound MnSOD indicates that product inhibition occurs when the peroxide complex becomes inner sphere. If the peroxide inhibits MnSOD by binding competitively to the same location as superoxide, then one can speculate that position 5 is where superoxide substrate binds during catalysis. Our structure shows that the active-site water (OH1) is displaced by peroxide binding and supports the associative-displacement mechanism proposed by Whittaker and Whittaker in 1996.¹⁸

Database accession numbers

Structure factors and atomic coordinates for the peroxide-soaked *E. coli* MnSOD crystals have been deposited in the Research Collaboratory for Structural Bioinformatics PDB with accession number 3K9S.

Acknowledgements

The authors would like to thank David Silverman for helpful and insightful discussion. This work was supported by NASA grants NAG-1380 and NAG8-1825.

References

- McCord, J. M. (2002). Superoxide dismutase in aging and disease: an overview. *Methods Enzymol.* **349**, 331–341.
- Perry, J. J., Fan, L. & Tainer, J. A. (2007). Developing master keys to brain pathology, cancer and aging from the structural biology of proteins controlling reactive oxygen species and DNA repair. *Neuroscience*, **145**, 1280–1299.
- Deng, H. X., Hentati, A., Tainer, J. A., Iqbal, Z., Cayabyab, A., Hung, W. Y. *et al.* (1993). Amyotrophic lateral sclerosis and structural defects in Cu,Zn superoxide dismutase. *Science*, **261**, 1047–1051.
- Rakhit, R. & Chakrabartty, A. (2006). Structure, folding, and misfolding of Cu,Zn superoxide dismutase in amyotrophic lateral sclerosis. *Biochim. Biophys. Acta*, **1762**, 1025–1037.
- Borgstahl, G. E., Parge, H. E., Hickey, M. J., Beyer, W. F., Jr., Hallewell, R. A. & Tainer, J. A. (1992). The structure of human mitochondrial manganese superoxide dismutase reveals a novel tetrameric interface of two 4-helix bundles. *Cell*, **71**, 107–118.
- Wagner, U. G., Patridge, K. A., Ludwig, M. L., Stallings, W. C., Werber, M. M., Oefner, C. *et al.* (1993). Comparison of the crystal structures of genetically engineered human manganese superoxide dismutase and manganese superoxide dismutase from *Thermus thermophilus*: differences in dimer-dimer interaction. *Protein Sci.* **2**, 814–825.
- Edwards, R. A., Baker, H. M., Whittaker, M. M., Whittaker, J. W., Jameson, G. B. & Baker, E. N. (1998). Crystal structure of *Escherichia coli* manganese superoxide dismutase at 2.1 Å resolution. *J. Biol. Inorg. Chem.* **3**, 161–171.
- Bannister, W. H. & Bannister, J. V. (1987). Factor analysis of the activities of superoxide dismutase, catalase, and glutathione peroxidase in normal tissues and neoplastic cell lines. *Free Radical Res. Commun.* **4**, 1–13.
- Holm, R. H., Kennepohl, P. & Solomon, E. I. (1996). Structural and functional aspects of metal sites in biology. *Chem. Rev.* **96**, 2239–2314.
- Fee, J. A. & Bull, C. (1986). Steady-state kinetic studies of superoxide dismutases. Saturative behavior of the copper- and zinc-containing protein. *J. Biol. Chem.* **261**, 13000–13005.
- Bull, C., Niederhoffer, E. C., Tatsuuro, Y. & Fee, J. A. (1991). Kinetic studies of superoxide dismutases: properties of the manganese-containing protein from *Thermus thermophilus*. *J. Am. Chem. Soc.* **113**, 4069–4076.
- Hearn, A. S., Stroupe, M. E., Cabelli, D. E., Lepock, J. R., Tainer, J. A., Nick, H. S. & Silverman, D. N. (2001). Kinetic analysis of product inhibition in human manganese superoxide dismutase. *Biochemistry*, **40**, 12051–12058.
- Hearn, A. S., Tu, C., Nick, H. S. & Silverman, D. N. (1999). Characterization of the product-inhibited complex in catalysis by human manganese superoxide dismutase. *J. Biol. Chem.* **274**, 24457–24460.
- Zheng, J., Domsic, J. F., Cabelli, D., McKenna, R. & Silverman, D. N. (2007). Structural and kinetic study of differences between human and *Escherichia coli* manganese superoxide dismutases. *Biochemistry*, **46**, 14830–14837.
- Lah, M. S., Dixon, M. M., Patridge, K. A., Stallings, W. C., Fee, J. A. & Ludwig, M. L. (1995). Structure-function in *Escherichia coli* iron superoxide dismutase: comparisons with the manganese enzyme from *Thermus thermophilus*. *Biochemistry*, **34**, 1646–1660.
- Ludwig, M. L., Metzger, A. L., Patridge, K. A. & Stallings, W. C. (1991). Manganese superoxide dismutase from *Thermus thermophilus*: a structural model refined at 1.8 Å resolution. *J. Mol. Biol.* **219**, 335–358.
- Tierney, D. L., Fee, J. A., Ludwig, M. L. & Penner-Hahn, J. E. (1995). X-ray absorption spectroscopy of the iron site in *Escherichia coli* Fe(III) superoxide dismutase. *Biochemistry*, **113**, 1661–1668.

18. Whittaker, M. M. & Whittaker, J. W. (1996). Low temperature thermochromism marks a change in coordination for the metal ion in manganese superoxide dismutase. *Biochemistry*, **35**, 6762–6770.
19. Borgstahl, G. E., Pokross, M., Chehab, R., Sekher, A. & Snell, E. H. (2000). Cryo-trapping the six-coordinate, distorted-octahedral active site of manganese superoxide dismutase. *J. Mol. Biol.* **296**, 951–959.
20. Shin, D. S., Didonato, M., Barondeau, D. P., Hura, G. L., Hitomi, C., Berglund, J. A. *et al.* (2009). Superoxide dismutase from the eukaryotic thermophile *Alvinella pompejana*: structures, stability, mechanism, and insights into amyotrophic lateral sclerosis. *J. Mol. Biol.* **385**, 1534–1555.
21. Otwinowski, Z. & Minor, W. (1997). Processing of X-ray diffraction data collected in oscillation mode. *Methods Enzymol.* **276**, 307–326.
22. Murshudov, G. N., Vagin, A. A. & Dodson, E. J. (1997). Refinement of macromolecular structures by the maximum-likelihood method. *Acta Crystallogr., Sect. D: Biol. Crystallogr.* **53**, 240–255.
23. Laskowski, R. A., MacArthur, M. W., Moss, D. S. & Thornton, J. M. (1993). PROCHECK: a program to check the stereochemical quality of protein structures. *J. Appl. Crystallogr.* **26**, 283–291.
24. Emsley, P. & Cowtan, K. (2004). Coot: model-building tools for molecular graphics. *Acta Crystallogr., Sect. D: Biol. Crystallogr.* **60**, 2126–2132.
25. Kleywegt, G. J. & Jones, T. A. (1997). Model building and refinement practice. *Methods Enzymol.* **277**, 208–230.
26. Kitajima, N., Komatsuzaki, H., Hikichi, S., Osawa, M. & Moro-oka, Y. (1994). A monomeric side-on peroxo manganese(III) complex: $\text{Mn}(\text{O}_2)(3,5\text{-iPr}_2\text{pzH})(\text{HB}(3,5\text{-iPr}_2\text{pz})_3)$. *J. Am. Chem. Soc.* **116**, 11596–11597.
27. VanAtta, R. B., Strouse, C. E., Hanson, L. K. & Valentine, J. S. (1987). [Peroxotetraphenylporphinato] manganese(III) and [chlorotetraphenylporphinato] manganese(II) anions. Syntheses, crystal structures, and electronic structures. *J. Am. Chem. Soc.* **109**, 1425–1434.
28. Guan, Y., Hickey, M. J., Borgstahl, G. E., Hallewell, R. A., Lepock, J. R., O'Connor, D. *et al.* (1998). Crystal structure of Y34F mutant human mitochondrial manganese superoxide dismutase and the functional role of tyrosine 34. *Biochemistry*, **37**, 4722–4730.
29. Cabelli, D. E., Guan, Y., Leveque, V., Hearn, A. S., Tainer, J. A., Nick, H. S. & Silverman, D. N. (1999). Role of tryptophan 161 in catalysis by human manganese superoxide dismutase. *Biochemistry*, **38**, 11686–11692.
30. Ren, X. L., Tu, C. K., Bhatt, D., Perry, J. J. P., Tainer, J. A., Cabelli, D. E. & Silverman, D. N. (2006). Kinetic and structural characterization of human manganese superoxide dismutase containing 3-fluorotyrosines. *J. Mol. Struct.* **790**, 168–173.